RESEARCH ARTICLE | OCTOBER 09 2024

Hidden data recovery using reservoir computing: Adaptive network model and experimental brain signals ⊘

Artem Badarin ⓘ ; Andrey Andreev ⓘ ; Vladimir Klinshov ⓘ ; Vladimir Antipov ⓘ ; Alexander E. Hramov ✉ ⓘ

⊙ Check for updates

View Online   Export Citation

Articles You May Be Interested In

Hidden data recovery using reservoir computing: Adaptive network model and experimental brain signals

Artem Badarin,[1] ID Andrey Andreev,[1] ID Vladimir Klinshov,[2,3] ID Vladimir Antipov,[1,3] ID
and Alexander E. Hramov[1,a] ID

AFFILIATIONS

[1] Baltic Center for Neurotechnology and Artificial Intelligence, Immanuel Kant Baltic Federal University, 236041 Kaliningrad,
Russia
[2] A. V. Gaponov-Grekhov Institute of Applied Physics of the Russian Academy of Sciences, 603155 Nizhny Novgorod, Russia
[3] Lobachevsky State University of Nizhny Novgorod, 603105 Nizhny Novgorod, Russia

[a] **Author to whom correspondence should be addressed:** hramovae@gmail.com

ABSTRACT

The problem of hidden data recovery is crucial in various scientific and technological fields, particularly in neurophysiology, where experimental data can often be incomplete or corrupted. We investigate the application of reservoir computing (RC) to recover hidden data from both model Kuramoto network system and real neurophysiological signals (EEG). Using an adaptive network of Kuramoto phase oscillators, we generated and analyzed macroscopic signals to understand the efficiency of RC in hidden signal recovery compared to linear regression (LR). Our findings indicate that RC significantly outperforms LR, especially in scenarios with reduced signal information. Furthermore, when applied to real EEG data, RC achieved more accurate signal reconstruction than traditional spline interpolation methods. These results underscore RC's potential for enhancing data recovery in neurophysiological studies, offering a robust solution to improve data integrity and reliability, which is essential for accurate scientific analysis and interpretation.

Published under an exclusive license by AIP Publishing. https://doi.org/10.1063/5.0223184

Machine learning, and more broadly artificial intelligence methods, are increasingly permeating various fields of natural sciences. They are also widely used in nonlinear dynamics and complex system theory for classifying dynamic operating modes of nonlinear systems, monitoring and controlling states of nonlinear systems, and predicting the behavior of chaotic oscillators, both concentrated self-sustained systems and spatially distributed chaotic systems. In this paper, we raise the question of the possibility of using such a machine learning technology as reservoir computing (RC) for the task of finding hidden data in complex networks. This is a typical situation when we have only part of the information about the dynamics of a complex network, for example, due to limitations in our data collection systems. This is typical for climate and weather problems, and such situations arise in brain research. Here, we investigate the application of reservoir computing to recover hidden data from both model Kuramoto network system and real neurophysiological signals.

We show that the potential of machine learning in such problems, based on data-driven approaches, is very high and surpasses standard methods that have been used to solve similar problems before.

I. INTRODUCTION

One of the important and urgent tasks arising in various scientific fields is the recovery of hidden data and patterns in experimentally investigated systems. Several research directions can be distinguished in this area. One of them is the recovery of hidden characteristics of the system to create more accurate models. For example, Kyoto Encyclopedia of Genes and Genomes (KEGG) mapping tools allow identifying hidden features in biological data, which significantly improves the accuracy and adequacy of models.[1] Another important direction is to augment the data based on the

identified system characteristics. This provides more complete and reliable data for further analysis.[2–4]

As an example from the field of neuroscience, we can highlight the problem of the possibility of spatial and temporal expansion of electroencephalographic (EEG) signals based on a few experimentally recorded signals. In Ref. 3, a convolutional neural network model was proposed for generating new signals of brain electrical activity to increase the density of electrode placement. Compared with standard spline interpolation methods, the authors show that the use of the neural network allows for achieving better results. In the paper,[2] a new neural network model was developed to recover original electroencephalographic (EEG) signals from noisy data in the presence of recording artifacts.

EEG is a method of recording electrical activity of the brain based on the measurement of potential differences on the scalp surface.[5] EEG signals are formed due to the combined activity of many neurons, mainly pyramidal cells of the cerebral cortex, which generate postsynaptic potentials. Mostly, brain electrical activity recorded by EEG electrodes represents synchronized activity of many neurons. This synchronized activity creates macroscopic electrical signals that propagate through the conductive tissues of the brain and skull. During the propagation, signals from different sources of neuronal activity are summarized. This causes each electrode to pick up integrated electrical activity from multiple sources. It means that the same source of neural activity can be registered by several electrodes. This fact makes it possible to recover signals from part of the electrodes by using others.

At the same time, the quality of EEG signal recording can vary during the experiment, which depends on many factors, including technical aspects, patient's condition, and external conditions.[6,7] The most common causes of signal degradation are poor contact between the electrodes and the scalp, electrode movement caused by head movement or the electrodes themselves, physiological artifacts (facial and neck muscle movements can create artifacts in EEG signals, such as artifacts from eye blinking or chewing), and others. Collectively, this leads to the fact that some data may be lost or only partially recorded, which causes the need to recover the lost data.

The recovery and analysis of macroscopic brain signals, such as EEG/MEG, are of paramount importance in biomedical and cognitive neuroscience research.[8–12] The significance of EEG stems from several key advantages. First, EEG is a non-invasive technique, making it safe and convenient for long-term monitoring of brain activity in patients.[13–15] This is particularly crucial in the diagnosis and treatment of neurological disorders such as epilepsy, where precise identification of pathological activity sources can significantly enhance treatment outcomes.[16] Second, EEG provides high temporal resolution, enabling the study of the temporal and spatial characteristics of neural activity during cognitive processes.[17–19] This high temporal resolution offers unique opportunities for gaining a deeper understanding of the intricate mechanisms underlying brain function. Third, EEG is a standard neuroimaging technique employed in brain–computer interfaces (BCIs) due to its simplicity and portability.[20] While BCIs typically utilize a limited number of EEG channels, augmenting these channels through machine learning techniques has emerged as a promising avenue for improving the quality of mental command recognition.[21,22] Therefore, advancements in methods for recovering and improving the quality of EEG

signals directly contribute to the creation of more accurate and reliable models. These models, in turn, have a profound impact on the development of novel technologies and treatment approaches in neurology, psychiatry, and cognitive neuroscience.[11,23]

One of the most effective methods to address this problem is leveraging artificial intelligence and machine learning, which have proven their utility in various fields, particularly when it comes to identifying hidden patterns in big data. When working with time series, reservoir computing (RC), a kind of recurrent neural network, is highly suitable and offers high efficiency.[24,25] RC has already demonstrated its simplicity and effectiveness in forecasting the dynamics of chaotic systems based on time series.[26,27] Notably, our studies have shown that using RC-based approaches enables the forecasting of macroscopic signals from adaptive Kuramoto networks.[28,29] Additionally, this method can forecast the coherent resonance observed in the Fitzhugh–Nagumo stochastic neuron.[30] Nevertheless, the application of RC in recovering hidden macroscopic signals from complex networks remains unexplored and holds substantial practical significance.

In this paper, we thoroughly examine the capabilities of RC in addressing the issue of recovering collective network dynamics. We explore an adaptive Kuramoto phase oscillator network where communication parameters between nodes are dynamically modulated based on their previous states.[31–33] Specifically, the strength of the link between nodes is determined by their degree of synchronization during the preceding time period. This implies that connections between oscillators are reinforced by synchronous behavior and weakened when their phases diverge. The network's adaptability allows for dynamic structural changes, forming clusters of synchronized oscillators. This emergent property is crucial for achieving high levels of system synchronization. This approach enables modeling the self-organization and adaptive capabilities observed in real neural systems in response to environmental changes or internal fluctuations.

It should be noted that a Kuramoto model stands as one of the most straightforward and widely used models for describing synchronization in systems comprising numerous oscillators.[34,35] It was specifically conceived to investigate synchronization phenomena that are also observed in neural networks within the brain.[36–38] Second, the Kuramoto network model enables us to elucidate how oscillators possessing distinct natural frequencies can synchronize via interaction, mirroring the dynamics of neurons in the brain.[35,37] Furthermore, the Kuramoto oscillator network and cortical networks exhibit macroscopic rhythms that stem from the collective behavior of multiple oscillators.[31,35,39–41] In the Kuramoto model, these rhythms emerge due to the phase synchronization of oscillators, which bears resemblance to the generation of brain rhythms (such as alpha, beta, theta rhythms, and others) registered in EEG/MEG signals.[42,43]

Importantly, adaptability plays a key role in maintaining and enhancing synchronized dynamics within the model, promoting the formation of stable clusters that are essential for the overall network function. This distinction makes our model more realistic than traditional Kuramoto models with fixed coupling parameters, incorporating features more characteristic of real biological systems.[44] We have previously utilized this model to study the characteristics of macroscopic signals associated with epileptic brain activity

10 October 2024 13:36:54

in an animal model of epilepsy.[45] Consequently, we believe that the Kuramoto adaptive oscillator network model provides a simplified framework for further comparison with the results of EEG signal reconstruction.

Initially, we simulate an adaptive Kuramoto oscillator network and generate M macroscopic signals, $M - 1$ of which are utilized to reconstruct the remaining one. We evaluate the quality of macroscopic signal recovery as a function of the degree of overlap between the macroscopic signals, encompassing scenarios where the macroscopic signals do not fully cover the whole network. In such cases, certain network elements are not directly incorporated into the macroscopic signals but exert an influence on them via interacting network elements. Then, we test the proposed RC-based approach on the real macroscopic signals of rest-state brain electrical activity measured by EEG.

The structure of the paper is as follows. In Sec. II, we consider the data that we use to analyze the RC's ability to reconstruct hidden variables. As such models, we use an adaptive Kuramoto network and an EEG dataset of resting-state data collected at the Immanuel Kant Baltic Federal University. In Sec. III, we consider a machine learning RC-based model and metrics that allow us to evaluate the recovery quality. We pay special attention to explaining the obtained results based on the analysis of mutual information in macroscopic signals. Finally, in Secs. IV and V, we discuss the obtained results, their limits of applicability, and directions for further research.

II. DATA UNDER STUDY

A. Adaptive Kuramoto network

As the model system, we use the network of Kuramoto phase oscillators proposed in Ref. 31 and analyzed in detail in Refs. 32 and 33. The network consists of $N_{osc} = 300$ phase oscillators and is described by the following equation:

$$\dot{\phi}_i(t) = \omega_i + \lambda \sum_{j \neq i} w_{ij}(t) \sin(\phi_j - \phi_i), \qquad (1)$$

where ϕ_i is the phase of the ith oscillator, $i = 1, \ldots, N_{osc}$, $\lambda = 1$ is a coupling strength, ω_i is a natural frequency, w_{ij} is the weight of the connection between ith and jth nodes, which is changed in time according to the adaptive rule,

$$\dot{w}_{ij}(t) = p_{ij}(t) - \left(\sum_{k \neq i} p_{ik}(t) \right) w_{ij}(t), \qquad (2)$$

where $p_{ij}(t)$ is defined as

$$p_{ij}(t) = \frac{1}{T_m} \left| \int_{t-T_m}^{t} \exp^{i(\phi_i(t') - \phi_j(t'))} dt' \right|. \qquad (3)$$

Here, $p_{ij}(t)$ denotes, at time t, the average phase correlation between oscillators i and j over a characteristic memory time $T_m = 15$. In this case, an additional condition is imposed on the dynamics of the weights w_{ij} that at any moment of time for each ith oscillator the set connection weights satisfies the condition corresponding to

homeostatic processes,[31]

$$\sum_{j \neq j}^{N_{osc}} w_{ij} = 1. \qquad (4)$$

To solve the system of integrodifferential equations (1)–(4), we use an approach based on the fourth-order Runge–Kutta method for the ordinary differential equation components and quadrature rules for the integral components[46] with a time step of $\Delta t = 0.01$. The initial conditions were the following: each ith node interacts with K randomly chosen neighboring nodes with strength $w_{ij} = 1/K$. The phases ϕ_i and frequencies ω_i are randomly selected in the interval $[-\pi, \pi]$. At the beginning of the calculations, we solved the system without adaptation with fixed coupling strength $w_{ij} = 1/K$, and after $t = 2T_m$ we turned on adaptation (2) and (3).

To describe the macroscopic dynamics of an adaptive Kuramoto network, we use the concept of macroscopic signals.[45] The process of forming groups and calculating macroscopic signals is illustrated in Fig. 1(a). We consider several macroscopic signals from different parts of the network. For this, we randomly categorize the oscillators into $M = 6$ groups (S_j, $j = 1, \ldots, M$) with equal number of elements (i.e., $M_{group} = N_{osc}/M = 50$ oscillators in each group). For all groups, the following condition imposed on each pair of groups is fulfilled $S_i \cap S_j = \varnothing$, where $i \neq j$.

The macroscopic signal for each group was defined as

$$X_j(t) = \frac{1}{M_{group}} \sum_{i \in S_j} \sin[\phi_i(t)]. \qquad (5)$$

To analyze the effect of the group intersection on a macroscopic signal recovery, we define the intersection rule as follows [see Fig. 1(b)]. Let us denote the result of selecting Δ random elements from the set S as $R(S, \Delta)$. Then, the set S_i^Δ with intersection equal to Δ is defined as

$$S_i^\Delta = \bigcup_{j=1, i \neq j}^{6} [S_i, R(S_j, \Delta)]. \qquad (6)$$

We also considered the scenario where the formed oscillator groups do not fully encompass the network. In such a case, we randomly eliminated δ elements from the initial set S [see Fig. 1(c)]. In other words, each set was constructed as follows:

$$S_i^\delta = S_i \setminus R(S_i, \delta). \qquad (7)$$

B. Experimental EEG signals

We use experimental data to analyze the possibility of using RC to restore one of the brain activity recording channels using information about other EEG recording channels. For this purpose, we use two-minute recordings of the background electrical activity of the brain in the rest-state with open eyes recorded in healthy subjects. An electroencephalograph "actiCHamp" manufactured by Brain Products, Germany, was used to record EEG activity. EEG signals were recorded for 63 channels according to the "10–10" scheme with a sampling frequency of 1000 Hz. We used minimal preprocessing to reconstruct the EEG signals. The EEG data were filtered in the range [1, 40] Hz using a finite impulse response (FIR) filter.
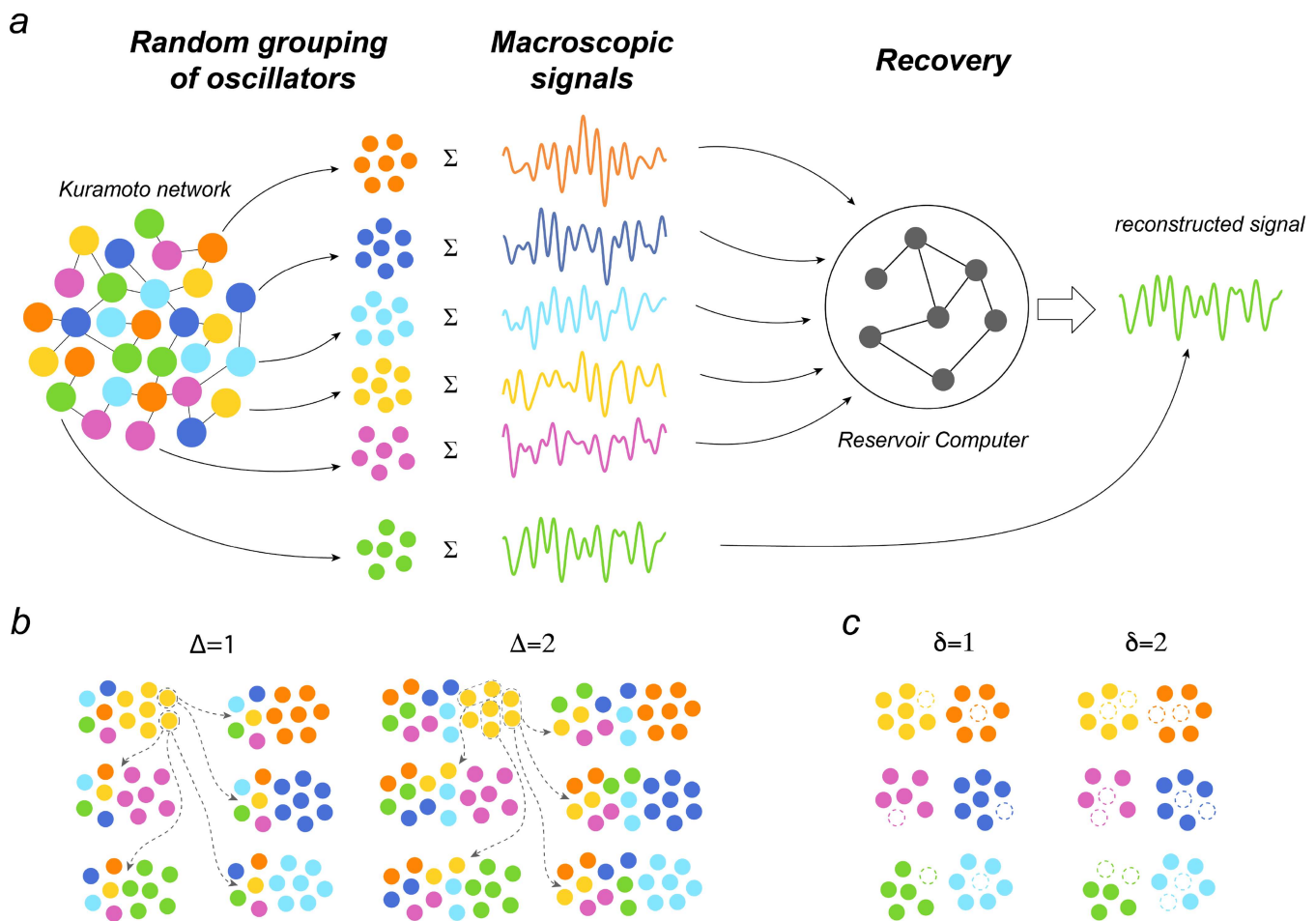
FIG. 1. Schematic representation of the Kuramoto oscillator network and the process of macroscopic signal formation. The colors here indicate groups of oscillators randomly assigned to one of six groups, each of which forms a macroscopic signal. (a) The network is randomly divided into $M = 6$ non-intersecting groups of oscillators. M macroscopic signals are formed from these groups, $M - 1$ of which are fed into the reservoir and used to reconstitute the remaining signal (light green). In this configuration, the RC has $M_{input} = M - 1$ macroscopic signals as input, and the output consists of a single reconstructed macroscopic signal. (b) The process of creating groups with common elements is visualized by a dashed arrow indicating elements randomly selected from the first group and added to other groups. Δ indicates the number of elements added to each group. (c) The process of erasing elements from groups. δ indicates the number of elements to be deleted from each group.

Twenty-three healthy subjects (11 males and 12 females) aged from 18 to 26 participated in the experiments. All of them provided written informed consent in advance. The experimental studies were performed by the Declaration of Helsinki and approved by the local Research Ethics Committee of Immanuel Kant Baltic Federal University (Protocol No. 32, 04.07.2022).

We designated one EEG channel as a hidden channel to reconstruct it using data from the remaining EEG channels. To achieve this, the first minute of recording was utilized as a training set to train the output layer of the RC, while data from the second minute were used to evaluate it. This procedure was iteratively applied to each EEG channel. Additionally, we optimized the RC hyperparameters for each recovered channel individually, aiming to minimize the reconstruction error for each subject's data.

III. RESERVOIR COMPUTING-BASED METHOD FOR HIDDEN DATA RECOVERY

A. Reservoir computing

In the classical application of RC to predict the behavior of dynamical systems,[26,27,47] including the macroscopic dynamics of an adaptive network,[28] the RC typically has an equal number of inputs and outputs. The hidden layer network (the reservoir itself) is randomly generated, and the weights of the output layer are selected during training to minimize a loss function. In the prediction mode, the output values are fed back into the input of the trained RC to predict new values of the analyzed process.

However, the RC architecture employed for the hidden variable recovery problem under consideration deviates from this classical

approach. When working with M macroscopic signals, we select one signal for reconstruction and use the remaining $M - 1$ signals as a basis for recovery. In this configuration, the RC has $M_{input} = M - 1$ macroscopic signals as input, and the output consists of a single reconstructed macroscopic signal as shown in Fig. 1(a). The internal state of this RC can be described as follows:

$$\mathbf{r}_{i+1} = (1 - l_r)\mathbf{r}_i + \tanh\left(\mathbf{W}_{reservoir}\mathbf{r}_i + \mathbf{W}_{input}\mathbf{X}_i\right) l_r, \quad (8)$$

where $\mathbf{r}_i$ is the vector of RC states in time moment i, $\mathbf{W}_{reservoir}$ is the matrix $N_{reservoir} \times N_{reservoir}$ of internal weights of RC, $N_{reservoir} = 100$ is the number of artificial neurons in the reservoir layer, $\mathbf{W}_{input}$ is the input weight matrix $(M - 1) \times N_{reservoir}$, $\mathbf{X}_i = \left[X_i^1, \ldots, X_i^{M-1}\right]^T$ is the vector of input signal in time moment i, and l_r is the leaking rate, which is the parameter that determines the extent to which previous states influence the current state. The input weight matrix $\mathbf{W}_{input}$ is randomly generated based on the parameter C_{input}, which specifies the probability of a link establishing between each input and reservoir neuron. The internal weights of the reservoir $\mathbf{W}_{reservoir}$ are generated randomly using a Bernoulli distribution and depend on the density of the internal reservoir matrix $C_{reservoir}$ and the spectral radius R. The density determines the probability of non-zero entries in the matrix $\mathbf{W}_{reservoir}$, which are sampled from a normal distribution, while the spectral radius normalizes the eigenvalues so that their maximum absolute value is equal to R.

The single output signal Y_i is derived by applying a linear transformation to the reservoir's internal state vector $\mathbf{r}_i$, following the relationship:

$$Y_i = \mathbf{W}_{out}\mathbf{r}_i, \quad (9)$$

where $\mathbf{W}_{out}$ is the output $N_{reservoir}$-component column vector. $\mathbf{W}_{out}$ is a vector and not a matrix due to the fact that the number of reservoir outputs is one, and output signal corresponds to a single recovery signal Y.

To determine the output weights of the RC, we compare the RC output $\mathbf{r}$ of size $N_{reservoir} \times L_{train}$ to the true signal $\mathbf{Y} = [Y_1, Y_2, .., Y_{L_{train}}]$ and calculate the output weights out $\mathbf{W}_{out}$ using the least squares method with Tikhonov regularization. Here, L_{train} is the training length. Consequently, $\mathbf{W}_{out}$ is defined as follows:

$$\mathbf{W}_{out} = \mathbf{Y}\mathbf{r}^T\left(\mathbf{r}\mathbf{r}^T + \eta\mathbf{I}\right)^{-1}. \quad (10)$$

Here, the regularization parameter is denoted by $\eta = 10^{-6}$ and $\mathbf{I}$ represents the identity matrix.

In the case of the adaptive Kuramoto network under study, after the formation of M macroscopic signals with specified parameters Δ and δ (see Sec. II A), one signal was randomly selected for reconstruction. The remaining $M - 1$ macroscopic signals served as a basis for recovery. The reservoir computer (RC) was provided with $M_{input} = M - 1$ macroscopic signals as input, producing a reconstructed version of the remaining macroscopic signal as output [see Fig. 1(a)]. The RC consisted of $N_{reservoir} = 100$ artificial neurons. For each parameter combination of δ and Δ, RC hyperparameter optimization was performed using random search[48] within the following ranges: l_r from 0.01 to 0.9; C_{input} and $C_{reservoir}$ from 0.05 to 0.9; R from 0.01 to 2. The random search algorithm was executed for 500 iterations. The optimization process minimized the total reconstruction error across ten randomly generated sets of six macroscopic signals for each unique δ and Δ combination. For each set, a random reservoir was created based on the optimized hyperparameters. The training phase utilized $L_{train} = 50\,000$ data points for training the output layer, followed by an additional 50 000 data points for testing the RC.

We utilized the ReservoirPy library for RC computations.[49]

B. Quality of recovery

To evaluate the accuracy of hidden macroscopic signal recovery, we calculated the relative error as follows:

$$Relative\ Error(Y^{rec}, Y) = \frac{Error\left(Y^{rec}, Y\right)}{Self\ Error}, \quad (11)$$

where

$$Error(Y^{rec}, Y) = \frac{\sum_i \left(Y_i^{rec} - Y_i\right)^2}{\sum_i \left(Y_i - \overline{Y}\right)^2}, \quad (12)$$

$$Self\ Error = \frac{1}{M - 1} \sum_{X_i \in \mathbf{S}_{input}} Error\left(X_i, Y\right). \quad (13)$$

Here, Y^{rec} is the recovery signal, Y is the true signal, M is the number of macroscopic signals, and $\mathbf{S}_{input}$ is the input set of macroscopic signals X_i.

C. Mutual information

To estimate the amount of information contained in the macroscopic signals fed into the RC, we used the average normalized value of the mutual information between the input macrosignals and the recovered signal (true signal),

$$MI = \frac{1}{M - 1} \sum_{X_i \in S_{input}} \frac{I(X_i, Y)}{H(Y)}, \quad (14)$$

where $I(X_i, Y) = H(X_i) + H(Y) - H(X_i, Y)$ is the mutual information between two signals, $H(X_i)$ and $H(Y)$ are the entropies of signals, and $H(X_i, Y)$ is the mutual entropy of signals.

To compute mutual information, we used the sklearn library, which implements a method based on entropy estimation via distances to k-nearest neighbors described in Refs. 50 and 51.

IV. RESULTS

A. Mutual information

The feasibility of recovering hidden data from available data hinges on the presence of a discernible relationship between the two data sets. One method for quantifying the strength of this relationship is to calculate the mutual information between the given data sets. In this study, we have investigated the impact of macroscopic signals, characterized by parameters Δ and δ, on the level of mutual information between them, as illustrated in Fig. 2. In Sec. IV B, we will use the mutual information between macroscopic signals to interpret the results of macroscopic signal reconstruction.

It is important to note that the formation of macroscopic signals involves an element of randomness. Specifically, we randomly
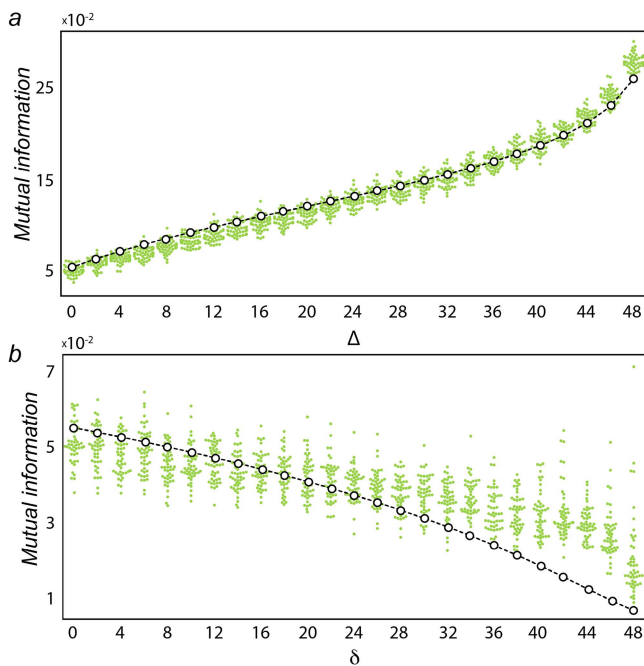
FIG. 2. Dependence of mutual information between macroscopic signals normalized by the entropy on the parameters of formed macroscopic signals. (a) Mutual information vs the number of signals added to the sets Δ. (b) Mutual information vs the number of signals erased from the sets δ. The green dots represent the results of the modeling, while the circles, connected by a dashed line, illustrate the analytical evaluation $I(Y_k, Y_m)/H(Y_k)$ [see Eq. (23)]. It should be noted that we fitted the free parameters in Eq. (23), such as D, d, and N_c, using the least squares method to compare the analytical estimation and the data.

select $N_{osc}/M = 50$ unique Kuramoto signals to contribute to each macroscopic signal (see Sec. II A for details). The resulting mutual information values are represented by the green dots in Fig. 2. It is well seen that increasing Δ, which is responsible for the presence of common elements in the macroscopic signals, leads to an increase in the mutual information between the macroscopic signals [see Fig. 2(a)]. At the same time, removing elements from the sets (increasing δ) decreases the mutual information [see Fig. 2(b)].

In order to understand the observed dependence between the mutual information and the parameters Δ and δ, we considered a toy model that admits analytic investigation. Recall that the typical collective regime of (1) is cluster synchronization.[31] Keeping this in mind, let us consider n units (oscillators) divided into N_c clusters of the equals size n/N_c, so that the output of the ith unit x_i is given as

$$x_i = X_j + \sigma_i, \tag{15}$$

where X_j is the (average) output of the jth cluster to which the unit belongs, and σ_i is the deviation. For simplicity, we assume that the outputs of the clusters are normally distributed and independent of each other, and the deviations are also normally distributed and independent: $X_j \sim N(0, D)$, $\sigma_j \sim N(0, d)$.

Now, let us divide the oscillator evenly into M groups $S_k = i_1^k, i_2^k, \ldots, i_s^k$ regardless of the cluster membership and then

introduce either intersection Δ or elimination δ in the way described by Eqs. (6) and (7), respectively. Then, the size of each group is given as

$$s = \begin{cases} \dfrac{n}{M} + (M-1)\Delta & \text{if } \Delta \geq 0, \\ \dfrac{n}{M} - \delta & \text{if } \delta > 0. \end{cases} \tag{16}$$

Let us define the output of each group as

$$Y_k = \frac{1}{s} \sum_{i \in S_k} x_i, \tag{17}$$

then the entropy of Y_k is given as

$$H(Y_k) = \frac{1}{2} \log 2\pi e D_Y, \tag{18}$$

where

$$D_Y = \frac{d}{s} + \frac{D}{N_c} \tag{19}$$

is the variance of the output.

The joint entropy of the outputs of two groups reads

$$H(Y_k, Y_m) = \log 2\pi e + \frac{1}{2} \log |\Sigma|, \tag{20}$$

where Σ is the covariance matrix with $\sigma_{11} = \sigma_{22} = D_Y$ and

$$\sigma_{12} = \sigma_{21} = \langle Y_k Y_m \rangle = \frac{r}{s^2} d + \frac{D}{N_c}, \tag{21}$$

where r is the number of common units in the two groups which can be estimated as

$$r = \begin{cases} \dfrac{\Delta^2 M(M-2)}{n} + 2\Delta & \text{if } \Delta \geq 0, \\ 0 & \text{if } \delta > 0. \end{cases} \tag{22}$$

Finally, we obtain

$$\begin{aligned} I &= H(Y_k) + H(Y_m) - H(Y_k, Y_m) \\ &= \log\left(\frac{d}{s} + \frac{D}{N_c}\right) - \frac{1}{2} \log\left[\frac{d^2}{s^2}\left(1 - \frac{r^2}{s^2}\right) + \frac{2dD}{sN_c}\left(1 - \frac{r}{s}\right)\right]. \end{aligned} \tag{23}$$

The analytical evaluation of the mutual information between the macroscopic signals of the network is represented in Fig. 2 by a dashed line with circles. It can be seen that the analytical dependencies obtained by proper choice of the parameters Δ and δ qualitatively and quantitatively reflect the main trends in the change of mutual information when increasing or decreasing data redundancy by adding or excluding elements (oscillators) from the groups.

Thus, both numerical simulations and analysis of the toy model show the presence of the information of some macroscopic signals of the network is contained in others, and this mutual information can be controlled by the intersection or elimination parameters. Further, we will study how efficiently this information can be extracted by different methods.

B. Data recovery

1. Model signals

To recover macroscopic signals, we consider and compare two approaches: multivariate linear regression (LR) and reservoir computing (RC). We analyze how efficiently each method can exploit the available data information. To this end, we examine the dependence of the relative recovery error on the mutual information. Note that we use the relative error to compensate for the effect of increasing similarity between macroscopic signals with increasing mutual information. To numerically characterize the degree of similarity between macrosignals, we introduce a characteristic that we termed
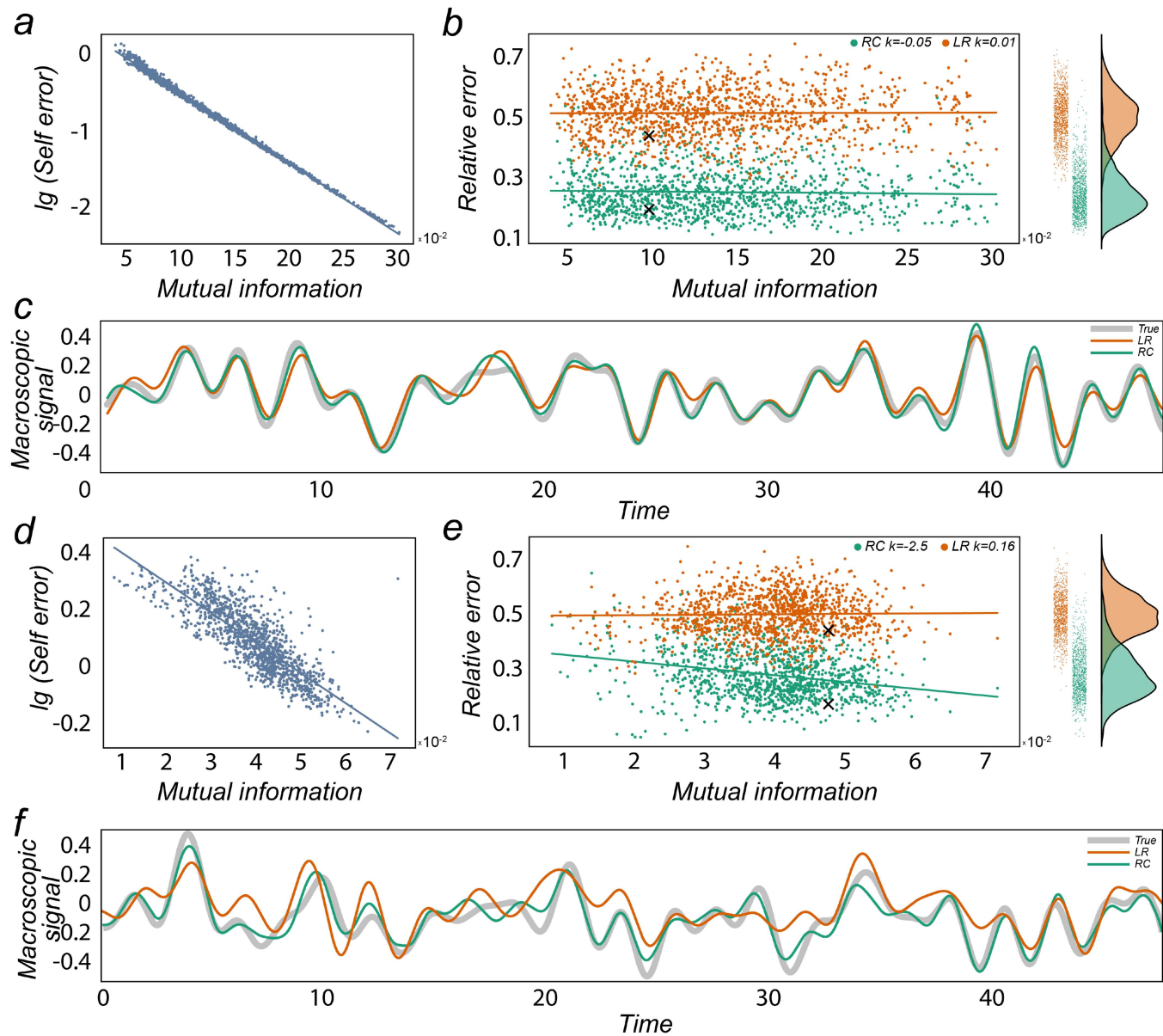
FIG. 3. Macroscopic signal recovery results. Panels (a)–(c) correspond to the case of adding common signals to the sets forming macroscopic signals ($\Delta > 0$), and panels (d)–(f) correspond to erasure from the sets of signals ($\delta > 0$). Panels (a) and (d) show the dependence of macroscopic signals self-error (13) on mutual information on a semi-logarithmic scale. (b) and (e) are the relative error (11) distributions for multivariate linear regression (orange dots) and RC (green dots). The lines correspond to the linear approximation of the distributions, and in the upper right corner, the corresponding slopes of the curves for each method are given. (c) and (f) correspond to temporal realizations of the recovered signals, and their corresponding values of mutual information and relative error are represented by crosses in the panels (b) and (e). Gray curves are the true signal, orange curves are LR-based recovery, and green curves are RC-based recovery.

self-error. From Fig. 3, we can clearly see that the increase in mutual information leads to an almost linear decrease in the self-error in semi-logarithmic scale, both for signals with intersection ($\Delta > 0$) and when erasing signals from the groups ($\delta > 0$). We use the self-error value as a baseline against which we analyzed the recovery error for each method.

As you can see from Figs. 3(b) and 3(e), the RC method significantly outperforms the LR method both when adding common signals $\Delta > 0$ and when erasing signals from the sets ($\delta > 0$). Indeed, the error for RC is about four times smaller than the baseline (true signals), whereas for LR the error is about three times smaller than the baseline.

We analyze the relationship between mutual information and relative error. For this purpose, we use a correlation analysis based on the Pearson correlation coefficient. It was found that there is no statistically significant correlation in the area of overlapping macroscopic signals [$\Delta > 0$, see Fig. 3(b)]. At the same time, when the signals are erased [$\delta > 0$, see Fig. 3(e)], there is a statistically significant correlation between mutual information and relative error for RC ($r = -0.254, p = 3.5 \times 10^{-19}$) but not for LR.

It should be noted that Figs. 3(c), and 3(f) show the time realizations of the reconstructed signals, and their corresponding values of mutual information and error are depicted by crosses in Figs. 3(b) and 3(e). From this figure, it is clearly seen that RC is better at recovering all the features of the macrosignal compared to LR. The qualitatively better prediction of the nonlinear model (RC) is especially good for the case $\delta > 0$, when we remove some information from the macroscopic signals. It is in this situation that the best ability of the reservoir to reveal hidden relationships for the recovery of hidden variables is well manifested.

To assess the generalizability of our findings, we investigated the impact of the number of macroscopic signals (M) on reconstruction accuracy for both methods under consideration (see Fig. 4). Our results indicate that, irrespective of the number of macroscopic signals, both methods demonstrate the ability to recover hidden data. Furthermore, increasing the number of macroscopic signals consistently leads to a reduction in the relative error. Notably, across all parameter values examined, RC consistently exhibits higher recovery accuracy compared to LR.

2. Experimental signals

We apply our developed approach to macroscopic signal recovery on real data of brain electrical activity recorded with EEG sensors [see Fig. 5(a)]. We found that, on average, using the RC method to reconstruct hidden channels outperforms the standard approach (spline interpolation) implemented in the widely used MNE package based on spline interpolation.[52] MNE package uses to reconstruct EEG signals spherical spline interpolation[53] based on the other EEG channels. This method creates a model of the electrical potential distribution on the head surface that projects sensor locations onto a unit sphere and interpolates the signal in needed sensor locations based on signals in other locations using Legendre polynomials. It should be notes that the spherical spline interpolation does not involve solving the inverse problem and restoring the sources of brain electrical activity, but only performs
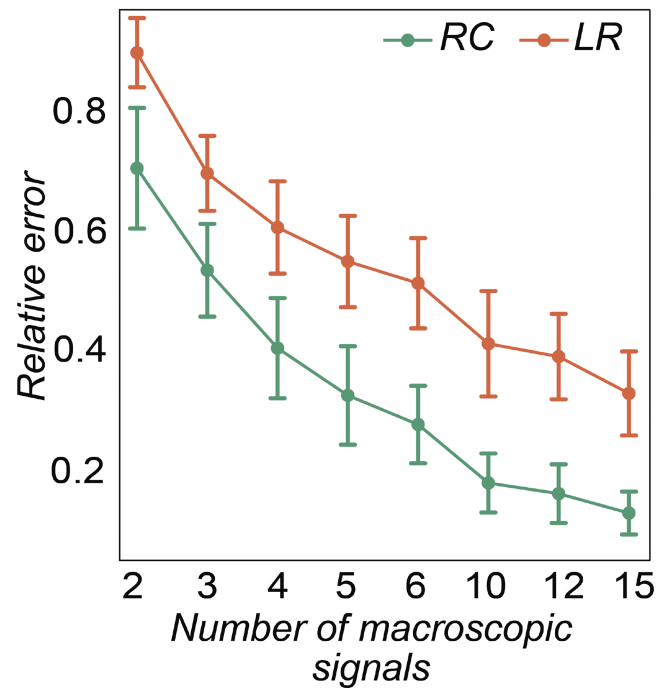

FIG. 4. Dependence of the relative error on the number of macroscopic signals at $\Delta = 0$ and $\delta = 0$. Here, the green and orange curves correspond to the RC and the LR recovery methods, respectively.

an instantaneous projection of the field distribution registered on good sensors onto bad channels.

Figure 5(b) shows the distribution of median values of relative recovery error ($Error_{MNE}/Error_{RC}$) over the head surface among 23 subjects. One can see that all the values obtained are greater than 1, with most of the values lying between 1 and 10. Moreover, in some cases, RC outperforms the standard approach by more than 40 times. At the same time, the distribution of the relative accuracy of channel recovery is not uniform over the head surface. In particular, there is a maximum difference between the methods in the frontal region and a minimum difference in the occipital region. It should be noted that the absolute accuracy of recovery also depends on the location of the channels: the best recovery results are observed in the central, frontal, and occipital regions, while more modest accuracy values are achieved in the temporal and parietal regions.

Figure 5(c) illustrates an example of applying EEG channel recovery methods. The left panel of Fig. 5(c) presents the time series of the P8 channel, located in the parietal lobe, along with reconstructions generated using the RC and LR methods, as well as the MNE package. The right panel of Fig. 5(c) shows the time-dependent recovery error for this signal, calculated in five-second windows for each method. As evident from Fig. 5(c), the error exhibits temporal fluctuations. However, across the entire time range, the RC-based method consistently achieves the lowest error.

Based on the data obtained, we systematically compared the performance of the LR and RC methods in reconstructing EEG
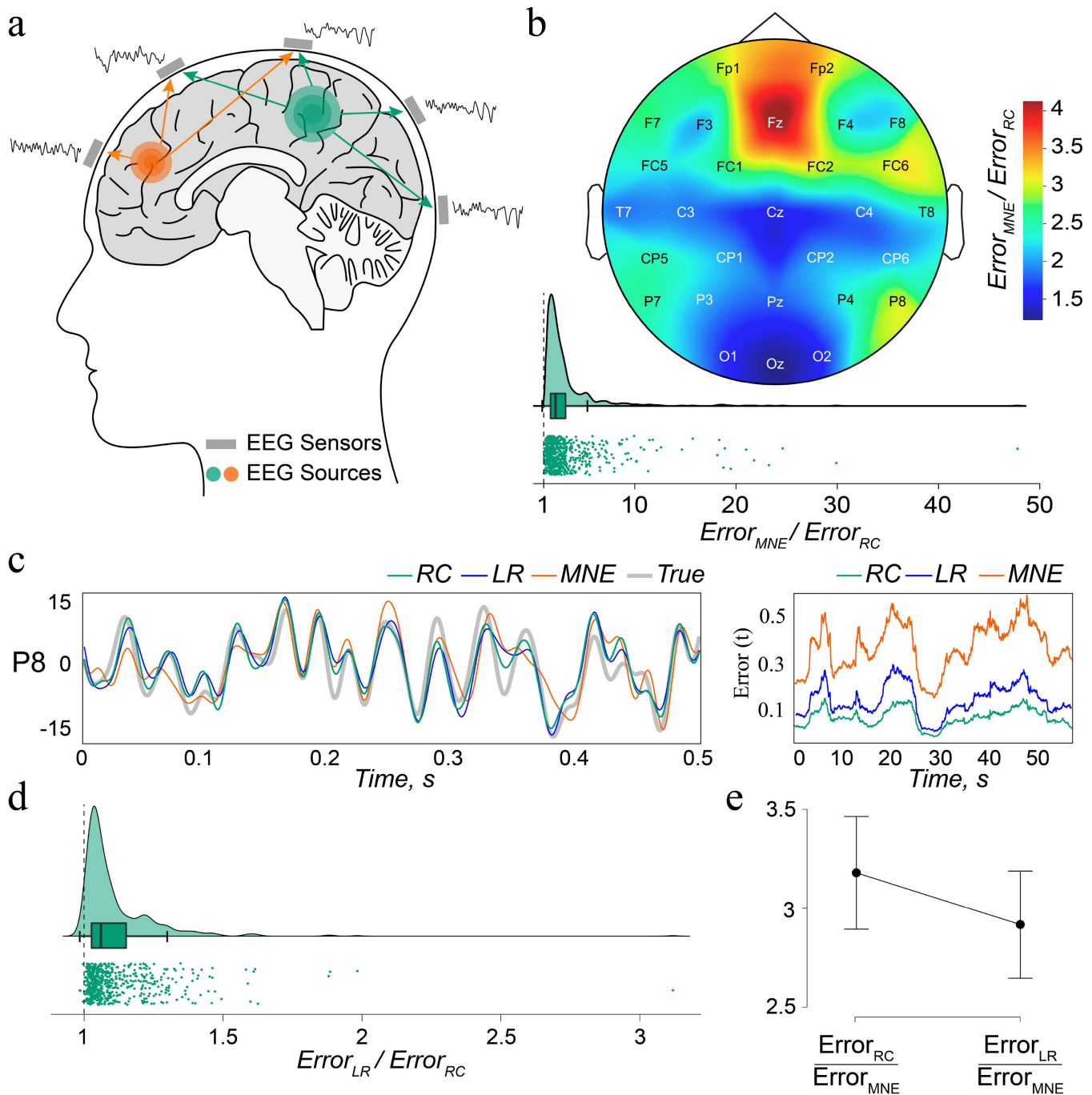
FIG. 5. Results of EEG channel reconstruction using RC and LR methods and standard approach implemented in MNE package based on the spline interpolation. (a) Schematic representation of sources in the brain whose activity is recorded by EEG sensors. (b) Distribution of median values of relationship $Error_{MNE}/Error_{RC}$ over the head surface among 23 subjects. The distribution of the recovery errors is shown below. Here, each point corresponds to the recovery results for all combinations of channels and subjects. (c) Gray curve is the example target signal for channel P8 from parietal lobe. Green, blue, and orange curves are reconstructed signals using RC and LR approaches and the MNE package, respectively. The time dependence of the recovery error calculated in a five-second time window for all methods used is shown on the right. (d) The distribution of the relative recovery errors for LR and RC approaches. (e) The mean and standard deviation for the recovery error for RC and LR approaches relative to the error obtained by the MNE package.

TABLE I. Spearman's rank correlations between the error ratio of the LR and RC methods, $Error_{LR}/Error_{RC}$, and the absolute error values for LR, RC, and MNE methods.

		Spearman's ρ	P value
$Error_{LR}/Error_{RC}$	$Error_{LR}$	0.313	2.148×10^{-15}
	$Error_{RC}$	0.246	6.124×10^{-10}
	$Error_{MNE}$	0.408	3.012×10^{-26}

signals [see Figs. 5(c) and 5(d)]. First, we analyzed the ratio of recovery errors, $Error_{LR}/Error_{RC}$, by using RC-based and LR-based methods for all EEG channels and participants. The distribution of this ratio, shown in Fig. 5(d), reveals that in most instances, the error ratio exceeds 1. This indicates that the RC-based method generally outperforms the LR-based method in terms of accuracy. Second, we compared the RC-based and LR-based methods with spherical spline interpolation, implemented in the MNE package [see Fig. 5(e)]. Our results demonstrate that both methods significantly outperform spherical spline interpolation. Third, a closer examination of the recovery errors revealed that the RC and LR methods exhibit comparable accuracy, both significantly superior to spherical spline interpolation. However, in certain cases, the accuracy of the RC method is notably higher than that of the LR method [see Fig. 5(e)].

We hypothesized that the RC-based method's superior performance in complex scenarios might be attributed to its ability to capture complex, nonlinear relationships between signals, which the LR-based method may struggle to represent. To prove this hypothesis, we conducted a correlation analysis. Given the potential presence of outliers and nonlinear dependencies in our data, we opted for Spearman's rank correlation coefficient, known for its robustness in such situations. We correlated the error ratio $Error_{LR}/Error_{RC}$ with the absolute error values for each method ($Error_{LR}$, $Error_{RC}$, and $Error_{MNE}$). The results of this analysis, presented in Table I, indicate a significant positive correlation between the error ratio and the errors for all methods considered. The strongest correlation was observed between $Error_{LR}/Error_{RC}$ and $Error_{MNE}$ ($\rho = 0.408$, $p = 3.012 \times 10^{-26}$).

Our findings suggest that in relatively straightforward cases, where recovery errors are minimal for all methods, the recovery errors of LR and RC approaches are similar. However, as the complexity of the reconstruction task increases, leading to higher errors across all methods, the RC method demonstrates significantly improved accuracy, further surpassing the LR method. This observation supports our hypothesis that the RC-based method excels in handling complex, nonlinear relationships within the data, contributing to its enhanced performance in more challenging scenarios.

V. DISCUSSION AND CONCLUSION

This study investigated the application of reconstructive coding (RC) for recovering hidden data within a model system and real neurophysiological signals, specifically electroencephalography (EEG).

Our model employed an adaptive network of Kuramoto phase oscillators to generate macroscopic signals through the superposition of signals from distinct oscillator groups. This network, with its carefully chosen parameters, exhibits self-organizing properties, leading to the spontaneous formation of synchronized clusters of oscillators from an initially random network.[31]

Our approach to the formation of macroscopic signals was based on the principle that each macroscopic signal comprises synchronized elements from multiple clusters within the network. This approach effectively reflects the diverse contributions of these elements to the overall signal. In our model, the number of elements from different clusters contributing to each macroscopic signal varied randomly. This diversity in contribution closely mirrors the formation of EEG signals, which arise from a heterogeneous mix of sources, including spatially distinct groups of neurons (analogous to clusters in the adaptive Kuramoto network) exhibiting synchronized dynamics. Just as different neuron groups contribute differentially to the EEG signal, elements from different clusters contribute with varying degrees to the macroscopic signal. Thus, our method of generating macroscopic signals from elements within the adaptive Kuramoto network provides a compelling representation of the process underlying the formation of macroscopic signals, such as EEG. It captures the complex and diverse contributions from different synchronized clusters, offering a valuable framework for understanding the intricate dynamics of these signals.

We investigated scenarios where groups forming macroscopic signals either fully encompassed the network, allowing for overlaps of Δ elements, or partially covered the network with factor δ without overlaps. We analyzed these macroscopic signals for mutual information content, observing that the addition of signals increased mutual information, while the removal of elements decreased it. These observations align closely with our qualitative analytical estimates. By varying the Δ and δ parameters, we generated sets of macroscopic signals with varying levels of mutual information. We assessed the impact of mutual information on the quality of model macroscopic signal recovery. Our findings indicate that RC more efficiently utilizes the available information for recovery than LR, with the recovery error for RC averaging half that of LR. We also conducted a correlation analysis to explore how mutual information levels affect recovery performance.

Our analysis revealed no significant correlation between the relative error and mutual information when common elements were added to the macroscopic signal sets, suggesting that both methods equally benefit from the increase in mutual information, which also leads to greater similarity among the macroscopic signals. However, when macroscopic signals were formed from a reduced number of elements in the original network (with element erasure, $\delta > 0$), indicating an information deficit about the system, a significant negative correlation was observed between the relative recovery error and mutual information for RC, but not for LR. This underscores RC's superior efficiency in leveraging additional information in the macroscopic signals. For LR, any increase in signal reconstruction accuracy was proportional to the increase in signal similarity. It should be noted that such a pattern in our opinion can be explained by the ability of RC to capture the non-linear relationship between macroscopic signals that manifested in the growth of mutual information but not captured by the LR method.

We investigated the impact of the number of macroscopic signals on the accuracy of hidden data recovery. Our findings demonstrate that increasing the number of partitions in the Kuramoto network, thereby forming a greater number of groups from which macroscopic signals are generated, leads to enhanced reconstruction accuracy. This improved accuracy arises from the fact that an increased number of macroscopic signals preserves more information about the overall network dynamics. This occurs because the averaging effect, which reduces information, is inversely proportional to the number of macroscopic signals. Consequently, a larger number of signals results in less averaging, leading to greater preservation of network information and, ultimately, improved reconstruction accuracy.

Thus, our investigation with modeled macroscopic signals demonstrated that the RC method can significantly outperform LR in recovering macroscopic signals. Moreover, while the LR method's recovery accuracy improvement correlates with an increase in signal similarity, RC excels under conditions of mutual information scarcity, achieving a more pronounced improvement in recovery accuracy than the corresponding increase in signal similarity.

One of the potential applications of macroscopic signal reconstruction is in the analysis of neurophysiological signals of different neuroimaging modalities. Neurophysiological experiments often encounter corrupted or lost data due to various reasons. Common causes of data corruption include noise from increased muscle tension as a result of experimental constraints or disruptions caused by the subject touching or scratching their head, potentially displacing electrodes, or causing significant signal interference.[6,7]

A common solution to these issues is data reconstruction using intact data. For EEG signals, spherical spline interpolation across neighboring, undamaged channels is frequently employed.[53,54] This method benefits significantly from the field spread effect, where electrical activity from the cortex, influenced by the brain tissue's uneven conductivity, may be detected more readily at neighboring electrodes rather than the closest one. This suggests that a single source may contribute to the signals at multiple electrodes, as illustrated in Fig. 5(a). However, spline interpolation does not account for individual anatomical differences, inaccuracies in electrode placement, or functional connections between different brain areas.[54]

After confirming that RC can effectively recover hidden data in model systems like Kuramoto phase oscillators and that RC not only reproduces macroscopic signals more accurately than linear methods but also captures hidden regularities we applied RC to real neurophysiological signals. We have compared different approaches for EEG data channel reconstruction including RC, LR, and spherical spline interpolation methods. The latter is implemented as a standard tool for EEG signal reconstruction in the MNE package.[52] Note that we did not test the spline interpolation approach on model data because the Kuramoto model network does not have a spatial arrangement of oscillators, and, hence, we could not use spherical spline interpolation for model data. Our results showed that RC performs, on average, 3.2 times better than the traditional approach, with some cases showing improvements up to 40-fold.

It is important to note that, unlike spherical spline interpolation, the proposed method for EEG channel recovery necessitates a training step for the output layer of the RC and requires access to a segment of undamaged data for this purpose. This requirement imposes certain limitations on the applicability of the proposed approach. Nonetheless, despite these constraints, the RC-based method can be highly beneficial for recovering individual epochs or fragments of EEG/MEG recordings that may be compromised due to physiological or technical artifacts. It is crucial to emphasize that many neurophysiological studies in clinical medicine and cognitive neuroscience rely on subjects repeatedly performing single-type tasks to elicit evoked or event-related potentials.[55–61] However, during the postprocessing of neurophysiological data, segments of EEG/MEG recordings that are damaged are frequently identified. Typically, these impaired fragments are either excluded from further analysis or interpolated, which—as a consequence of the repeated-measures design—can lead to data loss and diminished analysis quality. Specifically, the exclusion of individual epochs from the analysis can severely compromise the signal-to-noise ratio when studying evoked potentials, particularly when the number of events is limited.[59] In this context, the proposed RC-based recovery approach has the potential to significantly enhance the quality of data analysis in cognitive neuroscience, enabling more accurate interpretations of neurophysiological phenomena. Furthermore, it is plausible that we can train the model to recover data using a group of subjects, after which we can apply the RC model to restore data for an individual subject whose EEG/MEG recordings are compromised. However, this approach necessitates further analyses and experimentation to validate its effectiveness.

So, these findings underscore the substantial potential of RC in neurophysiological signal analysis. Nonetheless, it is important to recognize the additional limitations of our study. Our theoretical analysis was confined to a single model (the network of phase oscillators) and did not explore more realistic models. Future research will address this gap by applying our approach to spike neural networks and whole-brain models based on the models of neuronal masses.[62] Moreover, the influence of noise on data recovery remains unexplored. A significant constraint of our approach for real neurophysiological signals is the necessity for training data from areas with intact signals. Another limitation of our study is the specific focus on only one type of activity. Specifically, we trained and tested the RC approach using background activity alone. Consequently, this study did not explore the quality of signal recovery across different types of tasks. For instance, we did not evaluate the performance of our approach when using background recordings for training and then applying it to recover signals during the execution of experimental tasks, such as solving cognitive challenges. Special note, we observed that RC can identify latent interconnections between signals, highlighting the potential for developing new methods to restore functional relationships in neurophysiological data.

In conclusion, our study investigated the use of RC to recover hidden data from both model systems and real neurophysiological signals. We found that RC is twice as effective as LR in utilizing available signal information for recovery. Additionally, RC significantly outperforms the commonly used spline interpolation method in real neurophysiological data recovery tasks. These results demonstrate the strong potential of RC for both practical applications and basic research in neurophysiological signal analysis.

AUTHOR DECLARATIONS

Conflict of Interest

The authors have no conflicts to disclose.

Ethics Approval

Ethics approval for experiments reported in the submitted manuscript on animal or human subjects was granted. All participants provided written consent forms in accordance with the principles outlined in the Declaration of Helsinki. The study protocol received approval from the local Research Ethics Committee of Immanuel Kant Baltic Federal University (Protocol No. 32, 04.07.2022).

Author Contributions

Artem Badarin: Conceptualization (equal); Data curation (equal); Formal analysis (equal); Methodology (equal); Project administration (equal); Visualization (equal); Writing – original draft (equal). **Andrey Andreev:** Conceptualization (equal); Investigation (equal); Software (equal); Validation (equal); Visualization (equal); Writing – review & editing (equal). **Vladimir Klinshov:** Investigation (equal); Methodology (equal); Writing – original draft (equal). **Vladimir Antipov:** Formal analysis (equal); Software (equal); Validation (equal); Writing – review & editing (equal). **Alexander E. Hramov:** Conceptualization (equal); Formal analysis (equal); Funding acquisition (equal); Methodology (equal); Supervision (equal); Writing – original draft (equal).

DATA AVAILABILITY

The data that support the findings of this study are available from the corresponding author upon reasonable request.

REFERENCES

[1] M. Kanehisa, Y. Sato, and M. Kawashima, "KEGG mapping tools for uncovering hidden features in biological data," Protein Sci. **31**, 47–53 (2022).

[2] S. Mahmud, M. E. Chowdhury, S. Kiranyaz, N. Al Emadi, A. M. Tahir, M. S. Hossain, A. Khandakar, and S. Al-Maadeed, "Restoration of motion-corrupted EEG signals using attention-guided operational cyclegan," Eng. Appl. Artif. Intell. **128**, 107514 (2024).

[3] M. Svantesson, H. Olausson, A. Eklund, and M. Thordstein, "Virtual EEG-electrodes: Convolutional neural networks as a method for upsampling or restoring channels," J. Neurosci. Methods **355**, 109126 (2021).

[4] S. Zhang, H. Zhao, W. Wang, Z. Wang, X. Luo, A. Hramov, and J. Kurths, "Edge-centric effective connection network based on muti-modal MRI for the diagnosis of Alzheimer's disease," Neurocomputing **552**, 126512 (2023).

[5] P. L. Nunez and R. Srinivasan, *Electric Fields of the Brain: The Neurophysics of EEG* (Oxford University Press, 2006).

[6] X. Jiang, G.-B. Bian, and Z. Tian, "Removal of artifacts from EEG signals: A review," Sensors **19**, ' 987 (2019).

[7] J. A. Urigüen and B. Garcia-Zapirain, "EEG artifact removal—State-of-the-art and guidelines," J. Neural Eng. **12**, 031001 (2015).

[8] B. He, L. Yang, C. Wilke, and H. Yuan, "Electrophysiological imaging of brain activity and connectivity—Challenges and opportunities," IEEE Trans. Biomed. Eng. **58**, 1918–1931 (2011).

[9] V. Pizzella, L. Marzetti, S. Della Penna, F. de Pasquale, F. Zappasodi, and G. L. Romani, "Magnetoencephalography in the study of brain dynamics," Funct. Neurol. **29**, 241 (2014).

[10] A. Khosla, P. Khandnor, and T. Chand, "A comparative analysis of signal processing and classification methods for different applications based on EEG signals," Biocybern. Biomed. Eng. **40**, 649–690 (2020).

[11] Z. Wan, R. Yang, M. Huang, N. Zeng, and X. Liu, "A review on transfer learning in EEG signal analysis," Neurocomputing **421**, 1–14 (2021).

[12] A. Badarin, V. Antipov, V. Grubov, N. Grigorev, A. Savosenkov, A. Udoratina, S. Gordleeva, S. Kurkin, V. Kazantsev, and A. Hramov, "Psychophysiological parameters predict the performance of naive subjects in sport shooting training," Sensors **23**, 3160 (2023).

[13] T. D. Lagerlund, G. D. Cascino, K. M. Cicora, and F. W. Sharbrough, "Long-term electroencephalographic monitoring for diagnosis and management of seizures," in *Mayo Clinic Proceedings* (Elsevier, 1996), Vol. 71, pp. 1000–1006.

[14] L. Hellström-Westas and I. Rosén, "Continuous brain-function monitoring: State of the art in clinical practice," in *Seminars in Fetal and Neonatal Medicine* (Elsevier, 2006), Vol. 11, pp. 503–511.

[15] O. E. Karpov, V. V. Grubov, V. A. Maksimenko, S. A. Kurkin, N. M. Smirnov, N. P. Utyashev, D. A. Andrikov, N. N. Shusharina, and A. E. Hramov, "Extreme value theory inspires explainable machine learning approach for seizure detection," Sci. Rep. **12**, 11474 (2022).

[16] J. P. Koren, J. Herta, F. Fürbass, S. Pirker, V. Reiner-Deitemyer, F. Riederer, J. Flechsenhar, M. Hartmann, T. Kluge, and C. Baumgartner, "Automated long-term EEG review: Fast and precise analysis in critical care patients," Front. Neurol. **9**, 454 (2018).

[17] C. Babiloni, R. J. Barry, E. Başar, K. J. Blinowska, A. Cichocki, W. H. Drinkenburg, W. Klimesch, R. T. Knight, F. L. da Silva, P. Nunez *et al.*, "International federation of clinical neurophysiology (IFCN)—EEG research workgroup: Recommendations on frequency and topographic analysis of resting state EEG rhythms. Part 1: Applications in clinical research studies," Clin. Neurophysiol. **131**, 285–307 (2020).

[18] C. L. Wilkinson, L. D. Yankowitz, J. Y. Chao, R. Gutiérrez, J. L. Rhoades, S. Shinnar, P. L. Purdon, and C. A. Nelson, "Developmental trajectories of EEG aperiodic and periodic components in children 2–44 months of age," Nat. Commun. **15**, 5788 (2024).

[19] M. Seeber, L.-M. Cantonas, M. Hoevels, T. Sesia, V. Visser-Vandewalle, and C. M. Michel, "Subcortical electrophysiological activity is detectable with high-density EEG source imaging," Nat. Commun. **10**, 753 (2019).

[20] A. E. Hramov, V. A. Maksimenko, and A. N. Pisarchik, "Physical principles of brain–computer interfaces and their applications for rehabilitation, robotics and control of human brain states," Phys. Rep. **918**, 1–133 (2021).

[21] X. Gu, Z. Cao, A. Jolfaei, P. Xu, D. Wu, T.-P. Jung, and C.-T. Lin, "EEG-based brain-computer interfaces (BCIS): A survey of recent studies on signal sensing technologies and computational intelligence approaches and their applications," IEEE/ACM Trans. Comput. Biol. Bioinform. **18**, 1645–1666 (2021).

[22] S. Rasheed, "A review of the role of machine learning techniques towards brain–computer interface applications," Mach. Learn. Knowl. Extr. **3**, 835–862 (2021).

[23] F. L. da Silva, "EEG and MEG: Relevance to neuroscience," Neuron **80**, 1112–1128 (2013).

[24] G. Tanaka, T. Yamane, J. B. Héroux, R. Nakane, N. Kanazawa, S. Takeda, H. Numata, D. Nakano, and A. Hirose, "Recent advances in physical reservoir computing: A review," Neural Netw. **115**, 100–123 (2019).

[25] H. Jaeger, "The 'echo state' approach to analysing and training recurrent neural networks—With an erratum note," German National Research Center for Information Technology GMD Technical Report, Bonn, Germany (2001), Vol. 148, p. 13.

[26] D. J. Gauthier, E. Bollt, A. Griffith, and W. A. Barbosa, "Next generation reservoir computing," Nat. Commun. **12**, 1–8 (2021).

[27] J. Pathak, B. Hunt, M. Girvan, Z. Lu, and E. Ott, "Model-free prediction of large spatiotemporally chaotic systems from data: A reservoir computing approach," Phys. Rev. Lett. **120**, 024102 (2018).

[28]A. V. Andreev, A. A. Badarin, V. A. Maximenko, and A. E. Hramov, "Forecasting macroscopic dynamics in adaptive Kuramoto network using reservoir computing," Chaos **32**, 103126 (2022).

[29]A. Andreev, V. Antipov, and A. Badarin, "Using reservoir computing to predict a macroscopic signal," Bull. Russ. Acad. Sci.: Phys. **87**, 1523–1527 (2023).

[30]A. E. Hramov, N. Kulagin, A. V. Andreev, and A. N. Pisarchik, "Forecasting coherence resonance in a stochastic Fitzhugh–Nagumo neuron model using reservoir computing," Chaos, Solitons Fractals **178**, 114354 (2024).

[31]R. Gutiérrez, A. Amann, S. Assenza, J. Gómez-Gardenes, V. Latora, and S. Boccaletti, "Emerging meso-and macroscales from synchronization of adaptive networks," Phys. Rev. Lett. **107**, 234103 (2011).

[32]V. Makarov, A. Koronovskii, V. Maksimenko, A. Hramov, O. Moskalenko, J. M. Buldu, and S. Boccaletti, "Emergence of a multilayer structure in adaptive networks of phase oscillators," Chaos, Solitons Fractals **84**, 23–30 (2016).

[33]E. Pitsik, V. Makarov, D. Kirsanov, N. Frolov, M. Goremyko, X. Li, Z. Wang, A. Hramov, and S. Boccaletti, "Inter-layer competition in adaptive multiplex network," New J. Phys. **20**, 075004 (2018).

[34]J. A. Acebrón, L. L. Bonilla, C. J. P. Vicente, F. Ritort, and R. Spigler, "The Kuramoto model: A simple paradigm for synchronization phenomena," Rev. Mod. Phys. **77**, 137 (2005).

[35]F. A. Rodrigues, T. K. D. Peron, P. Ji, and J. Kurths, "The Kuramoto model in complex networks," Phys. Rep. **610**, 1–98 (2016).

[36]S. Zheng, Z. Liang, Y. Qu, Q. Wu, H. Wu, and Q. Liu, "Kuramoto model-based analysis reveals oxytocin effects on brain network dynamics," Int. J. Neural Syst. **32**, 2250002 (2022).

[37]R. Schmidt, K. J. LaFleur, M. A. de Reus, L. H. van den Berg, and M. P. van den Heuvel, "Kuramoto model simulation of neural hubs and dynamic synchrony in the human cerebral connectome," BMC Neurosci. **16**, 1–13 (2015).

[38]D. Cumin and C. Unsworth, "Generalising the Kuramoto model for the study of neuronal synchronisation in the brain," Phys. D: Nonlinear Phenom. **226**, 181–196 (2007).

[39]A. E. Hramov, A. A. Kharchenko, V. V. Makarov, M. V. Khramova, A. A. Koronovskii, A. N. Pavlov, and S. K. Dana, "Analysis of the characteristics of the synchronous clusters in the adaptive Kuramoto network and neural network of the epileptic brain," in *Saratov Fall Meeting 2015: Third International Symposium on Optics and Biophotonics and Seventh Finnish-Russian Photonics and Laser Symposium (PALS)* (SPIE, 2016), Vol. 9917, pp. 540–547.

[40]N. Frolov and A. Hramov, "Extreme synchronization events in a Kuramoto model: The interplay between resource constraints and explosive transitions," Chaos **31**, 063103 (2021).

[41]N. Frolov, V. Maksimenko, S. Majhi, S. Rakshit, D. Ghosh, and A. Hramov, "Chimera-like behavior in a heterogeneous Kuramoto model: The interplay between attractive and repulsive coupling," Chaos **30**, 081102 (2020).

[42]G. Buzsáki, *Rhythms of the Brain* (Oxford University Press, 2006).

[43]F. De Pasquale, S. Della Penna, A. Z. Snyder, C. Lewis, D. Mantini, L. Marzetti, P. Belardinelli, L. Ciancetta, V. Pizzella, G. L. Romani, and M. Corbetta, "Temporal dynamics of spontaneous MEG activity in brain networks," Proc. Natl. Acad. Sci. U.S.A. **107**, 6040–6045 (2010).

[44]D. Meunier, R. Lambiotte, and E. T. Bullmore, "Modular and hierarchically modular organization of brain networks," Front. Neurosci. **4**, 7572 (2010).

[45]V. A. Maksimenko, A. Lüttjohann, V. V. Makarov, M. V. Goremyko, A. A. Koronovskii, V. Nedaivozov, A. E. Runnova, G. van Luijtelaar, A. E. Hramov, and S. Boccaletti, "Macroscopic and microscopic spectral properties of brain networks during local and global synchronization," Phys. Rev. E **96**, 012316 (2017).

[46]A. Filiz, "A fourth-order robust numerical method for integro-differential equations," Asian J. Fuzzy Appl. Math. **1**, 23–33 (2013).

[47]A. Griffith, A. Pomerance, and D. J. Gauthier, "Forecasting chaotic systems with very low connectivity reservoir computers," Chaos **29**, 123108 (2019).

[48]J. Bergstra and Y. Bengio, "Random search for hyper-parameter optimization," J. Mach. Learn. Res. **13**, 281–305 (2012).

[49]N. Trouvain, L. Pedrelli, T. T. Dinh, and X. Hinaut, "Reservoirpy: An efficient and user-friendly library to design echo state networks," in *International Conference on Artificial Neural Networks* (Springer, 2020), pp. 494–505.

[50]B. C. Ross, "Mutual information between discrete and continuous data sets," PLoS One **9**, e87357 (2014).

[51]A. Kraskov, H. Stögbauer, and P. Grassberger, "Estimating mutual information," Phys. Rev. E **69**, 066138 (2004).

[52]A. Gramfort, M. Luessi, E. Larson, D. A. Engemann, D. Strohmeier, C. Brodbeck, R. Goj, M. Jas, T. Brooks, L. Parkkonen, and M. Hämäläinen, "MEG and EEG data analysis with MNE-python," Front. Neurosci. **7**, 70133 (2013).

[53]F. Perrin, J. Pernier, O. Bertrand, and J. F. Echallier, "Spherical splines for scalp potential and current density mapping," Electroencephalogr. Clin. Neurophysiol. **72**, 184–187 (1989).

[54]S. S. Kang, T. J. Lano, and S. R. Sponheim, "Distortions in EEG interregional phase synchrony by spherical spline interpolation: Causes and remedies," Neuropsychiatr. Electrophysiol. **1**, 1–17 (2015).

[55]K. H. Chiappa, "Evoked potentials in clinical medicine" 3rd ed. (Philadelphia, Lippincott-Raven, 1997).

[56]P. Walsh, N. Kane, and S. Butler, "The clinical role of evoked potentials," J. Neurol. Neurosurg. Psychiatry **76**, ii16–ii22 (2005).

[57]R. Henson, "What can functional neuroimaging tell the experimental psychologist?," Q. J. Exp. Psychol. Sec. A **58**, 193–233 (2005).

[58]B. Kotchoubey, "Event-related potentials, cognition, and behavior: A biological approach," Neurosci. Biobehav. Rev. **30**, 42–65 (2006).

[59]A. Mouraux and G. D. Iannetti, "Across-trial averaging of event-related EEG responses and beyond," Magn. Reson. Imaging **26**, 1041–1054 (2008).

[60]R. F. Helfrich and R. T. Knight, "Cognitive neurophysiology: Event-related potentials," Handb. Clin. Neurol. **160**, 543–558 (2019).

[61]A. N. Pisarchik, V. S. Khorev, A. A. Badarin, V. M. Antipov, A. O. Budarina, and A. E. Hramov, "Methodology of the neurophysiological experiments with visual stimuli to assess foreign language proficiency," Izv. Vys. Uch. Zav. Priklad. Neliney. Dinam. **31**, 202–224 (2023).

[62]G. Deco, V. K. Jirsa, P. A. Robinson, M. Breakspear, and K. Friston, "The dynamic brain: From spiking neurons to neural masses and cortical fields," PLoS Comput. Biol. **4**, e1000092 (2008).